Self-Assembly in Cells Hot Paper

How to cite: *Angew. Chem. Int. Ed.* **2021**, *60*, 23797–23804
International Edition: doi.org/10.1002/anie.202109729
German Edition: doi.org/10.1002/ange.202109729

Spatiotemporal Control over Chemical Assembly in Living Cells by Integration of Acid-Catalyzed Hydrolysis and Enzymatic Reactions

*Xuejiao Yang, Honglei Lu, Yinghua Tao, Laicheng Zhou, and Huaimin Wang**

Abstract: *Spatiotemporal control of chemical assembly in living cells remains challenging. We have now developed an efficient and general platform to precisely control the formation of assemblies in living cells. We introduced an O-[bis(dimethylamino)phosphono]tyrosine protection strategy in the self-assembly motif as the Trojan horse, whereby the programmed precursors resist hydrolysis by phosphatases on and inside cells because the unmasking of the enzymatic cleavage site occurs selectively in the acidic environment of lysosomes. After demonstrating the multistage self-assembly processes in vitro by liquid chromatography/mass spectrometry (LC-MS), cryogenic electron microscopy (Cryo-EM), and circular dichroism (CD), we investigated the formation of site-specific self-assembly in living cells using confocal laser scanning microscopy (CLSM), LC-MS, and biological electron microscopy (Bio-EM). Controlling chemical assembly in living systems spatiotemporally may have applications in supramolecular chemistry, materials science, synthetic biology, and chemical biology.*

Introduction

Molecular self-assembly[1] is a powerful strategy to construct functional structures of macromolecules with suitable folding and association in living cells. It is a widely used bottom-up approach to fabricate sophisticated structures in supramolecular chemistry, materials science, and medicinal chemistry. To control and direct the assembly of building blocks into functional nanostructures, external stimuli including pH adjustment, organic solvent assistance, light irradiation, sonication, and heating are usually employed.[2] Although exciting successes have been achieved in vitro, few of these strategies have been applied in vivo through in situ self-assembly, especially in living cells.

Enzymes are essential biomacromolecules that catalyze chemical reactions in nature. In the living system, the location and the activity of enzymes are precisely controlled to maintain cellular functions, such as cell proliferation, differentiation, migration, and aiding digestion and metabolism.[3] Inspired by the natural biochemical processes instructed by enzymes,[3] Xu and co-workers integrated an enzymatic reaction and noncovalent synthesis to construct supramolecular hydrogels in vitro and in vivo.[4] Over the last few years, it has become increasingly apparent that enzymatically induced self-assembly in living cells is an efficient strategy for controlling cell behaviors.[2c,5] For example, phosphatases have drawn much attention, largely because of their overexpression in cancer cells and low intrinsic substrate specificity, thereby making them a well-explored enzyme for inducing self-assembly.[6] Xu and co-workers reported the first case of using extracellular alkali phosphatase (ALP) to induce nanonet formation around a cancer cell membrane for cancer cell inhibition.[7] Ulijn and co-workers utilized a carbohydrate derivative to construct a hydrogel in situ by the cell-membrane-bound ALP.[5a] The Liang and Yang groups also reported the intracellular formation of nanofibers by tandem self-assembly that was initiated by extracellular ALP.[5c,f] Despite the achievements of using enzyme-instructed self-assembly to construct nanostructures in living systems, progress towards the precise formation of molecular assemblies has been limited and remains challenging,[8] because the precursors required for intracellular self-assembly will inevitably undergo hydrolysis by hydrolytic enzymes (e.g. phosphatase) with similar activities,[9] which results in nanostructure formation at unwanted times and in undesired locations.

The lysosome has been recognized as an essential cellular organelle (or recycling center) for the degradation and recycling of extracellular and intracellular materials.[10] Understanding of the lysosomal function and dysfunction in recent years has led to the suggestion that targeting lysosome selectively emerges as a novel opportunity for treating diseases. To demonstrate the concept, we aimed to take advantage of the acidic environment of the lysosome to remove the protecting group so that the acid phosphatase in the lysosome could instruct the self-assembly of the resulting hydrogelator spatiotemporally in the lysosome.

Here we reported an efficient and easily accessible strategy to precisely control the location of molecular assembly in living cells using multistage self-assembly. In this approach, we employed an *O*-[bis(dimethylamino)phosphono]tyrosine protection strategy[11] to avoid undesired enzymatic hydrolysis at the cell membrane and cytoplasm. As the hydrolysis of the P–N bond releases native phosphotyrosine under acidic conditions (Scheme S1), the enzyme-induced self-assembly would only be initiated in an acidic environment. Live cell studies show that the phosphoramidate group

[*] Dr. X. Yang, H. Lu, Y. Tao, L. Zhou, Prof. H. Wang
Key Laboratory of Precise Synthesis of Functional Molecules of Zhejiang Province, School of Science
Westlake University, Institute of Natural Sciences
Westlake Institute for Advanced Study
18 Shilongshan Road, Hangzhou 310024, Zhejiang Province (China)
E-mail: wanghuaimin@westlake.edu.cn
Prof. H. Wang
Westlake Laboratory of Life Sciences and Biomedicine
School of Life Sciences, Westlake University
Hangzhou, Zhejiang (China)
Supporting information and the ORCID identification number for one of the authors of this article can be found under: https://doi.org/10.1002/anie.202109729.

resists hydrolysis by ALP or other phosphatases at neutral pH. After being taken up by endocytosis, the phosphodiamidate building blocks undergo acid-catalyzed hydrolysis to yield the native substrate of the acid phosphatase (ACP) inside the lysosome to form oligomers,[12] which enables ACP to specifically induce the formation of nanofibrous networks inside the lysosome by removing the phosphate group. Thus, as the first example of controlling site-specific nanofiber formation through multistage self-assembly in living cells, this study illustrates a general strategy to precisely control nanostructure formation in living cells for the development of functional higher-order structures.

Results and Discussion

On the basis of the above concept, we rationally designed the precursor NBD-^{D}Wp^{D}Y(NMe$_2$)$_2$^{D}F^{D}K(Ac)-NH$_2$ (**Pro-1P-NMe**; Figure 1), which contains a phosphoramidate group for preventing enzymatic hydrolysis of phosphotyrosine at unwanted sites (i.e. on the cell membrane or inside the cytoplasm), a self-assembly motif consisting of tryptophan-tyrosine-phenylalanine (WYF) to provide the hydrogen bonding and aromatic–aromatic interactions. We chose the sequence of WYF since WY is a favorable amino acid composition at the protein–protein interface, which engages in hydrogen bonding and π-π stacking.[13] We utilized the acetylation of lysine since the protecting group could decrease the effect of electrostatic interactions. We also employed chloro-7-nitrobenzo-2,1,3-oxadiazole (NBD),[14] an environment-sensitive fluorophore, to visualize the cellular distribution of assemblies. Such a design allows the **Pro-1P-NMe** to be deprotected under acidic conditions and subsequently to release the precursor that is recognized by specific enzymes to trigger self-assembly. To synthesize the designed precursors, we first prepared tetrapeptide **1** through standard solid-phase (Fmoc) peptide synthesis (SPPS) using Rink-amide resin. We obtained the desired product by reacting **1** with *N*,*N*,*N*′,*N*′-tetramethylphosphorodiamidic chloride in 50% yield after purification by high-performance liquid chromatography (HPLC) and confirmed its structure by LC-MS and NMR spectroscopy (Scheme S1 and Figures S1, S2, and S15).

To characterize our designed multistage transformation, we first assessed the stability of **Pro-1P-NMe** at physiological pH values without or with the addition of enzymes. LC-MS spectra show that there is no degradation of **Pro-1P-NMe** after incubation for 72 h in aqueous buffer at pH 7.4 regardless of the presence of ALP or ACP (Figure 2A), which indicates that the phosphoramidate group could serve as a Trojan horse to protect phosphotyrosine against hydrolysis by phosphatase. In contrast, ALP converts almost 100% of NBD-^{D}Wp^{D}Y^{D}F^{D}K(Ac)-NH$_2$ (**1P**) to NBD-^{D}W^{D}Y^{D}F^{D}K(Ac)-NH$_2$ (**1**) within 30 min (Scheme S2 and Figures S3, S4, S16, and S22), in agreement with the previous report that phosphotyrosine is a nonspecific substrate for phosphatase.[15] These results also suggest that **Pro-1P-NMe** is stable in

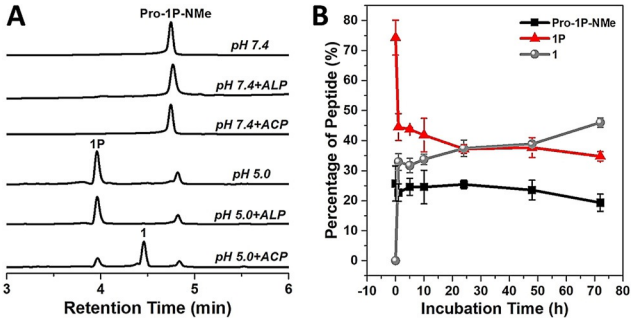

Figure 2. A) HPLC spectra of **Pro-1P-NMe** before and after incubation with ALP (3.0 U mL^{-1}) or ACP (0.1 U mL^{-1}) in aqueous buffer at different pH values. B) Hydrolysis ratio of **Pro-1P-NMe** incubated with ACP (0.1 U mL^{-1}) in aqueous solution at pH 5.0. The concentration of **Pro-1P-NMe** is 200 μM. The results were calculated from the HPLC spectra (Figure S24).

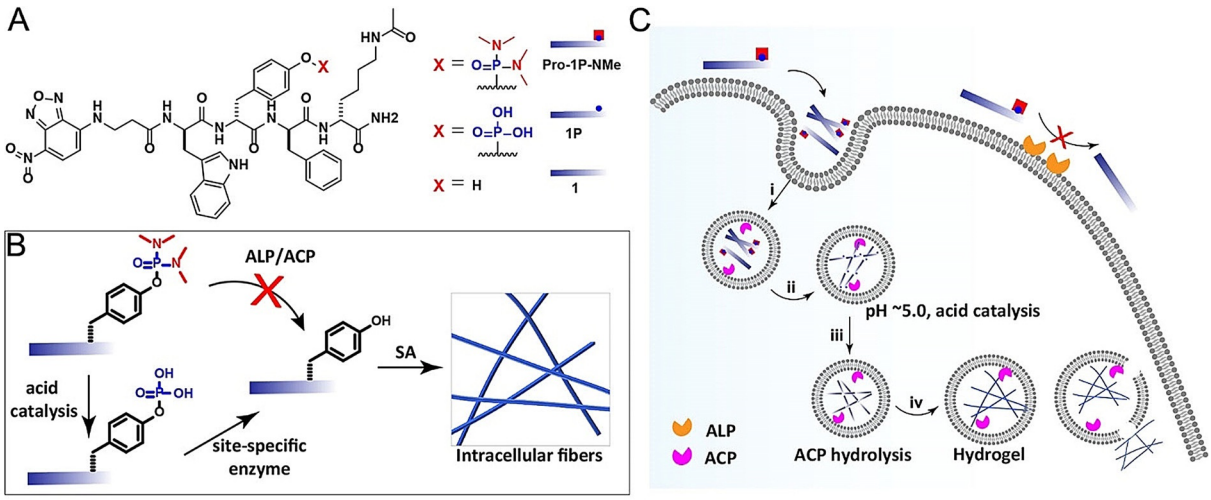

Figure 1. A) Molecular structures and B) illustration of multistage chemical reactions in vitro. C) Illustration of the site-specific construction of nanofibers in living cells through multistage processes: i) cellular uptake of molecules; ii) acid-catalyzed hydrolysis of the P–N bond of **Pro-1P-NMe** results in **1P** which forms oligomers; iii) acid phosphatase in the lysosome further induced hydrolysis of **1P** to **1**; and iv) self-assembly of **1** into an entangled nanofibrous network.

neutral environments (e.g. extracellular space, cell surface, or cytoplasm) that express phosphatase. Considering the pH range (6.5–6.8) in acid tumour environments[16] and lysosomes (5.0–6.0), we also investigated the stability of **Pro-1P-NMe** in an aqueous solution at pH 6.6. The results show that **Pro-1P-NMe** is quite stable at pH 6.6 (Figure S23), thus indicating the selective hydrolysis of **Pro-1P-NMe** in the lysosomal environment. Encouraged by these results, we next investigated the molecular transformation of **Pro-1P-NMe** at pH 5.0. LC-MS results reveal a new peak with a retention time of 3.96 min (74.3%), which corresponds to **1P** (Figures 2A,B and S24, S25, Table S2), as evident by the MS spectrum. Moreover, incubating above solution with ACP transforms **1P** to **1** (46.0%, Figure S26), whereas ALP results in no hydrolysis of **1P** under the same conditions (Figure 3A). To investigate the influence of the concentration of ACP on the rate of enzymatic hydrolysis we also used a higher concentration of ACP (1.0 U mL^{-1}) in the hydrolysis experiment. The results indicate that the enzyme remains active over the incubation time, and the formed nanostructure could prevent hydrolysis of the enzyme at the lower concentration of ACP (Figure S27). These results indicate that **Pro-1P-NMe** could sequentially transform into **1P** and **1** only in the presence of ACP in an acidic environment, thus suggesting that we could control the enzyme-instructed self-assembly at the site where the enzyme exists.

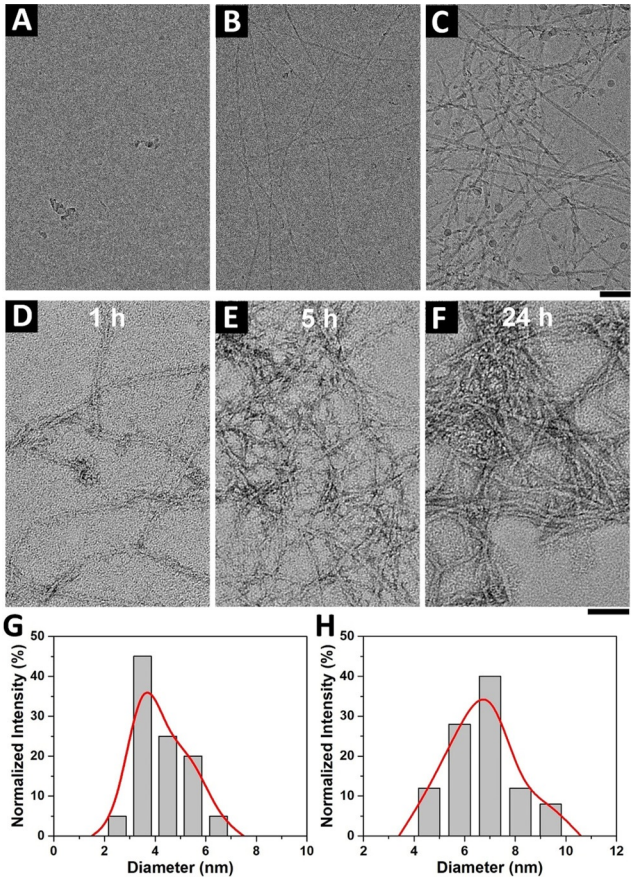

Figure 3. Cryo-EM images of **Pro-1P-NMe** incubated in aqueous solution at A) pH 7.4, B) pH 5.0, and C) 72 h after the addition of ACP (pH 5.0). Time-dependent TEM images of **Pro-1P-NMe** incubated with ACP at pH 5.0 for D) 1 h, E) 5 h, and F) 24 h. The concentration of the peptide and ACP is 200 μM and 0.1 U mL^{-1}, respectively. The scale bar in Figure 3A–F is 50 nm. Statistical average diameter of the nanofibers G) in Figure 3B, and H) in Figure 3C.

To investigate the multistage transformation of **Pro-1P-NMe** and their corresponding self-assembly morphologies at different stages, we performed cryogenic transmission electron microscopy (cyro-TEM). As shown in Figure 3, **Pro-1P-NMe** hardly forms any observable nanostructures at pH 7.4—we could only find a few dot-like structures in the TEM images (Figures 3A, S28). However, after incubating for 5 h in aqueous solution (pH 5.0), **Pro-1P-NMe** forms short and discrete nanofibers (Figure S29). The short nanofibers became longer as the incubation time increased to 10 h but the morphology hardly changed with further incubation (monitored at 24 h and 48 h), which indicates that the **1P** obtained from **Pro-1P-NMe** only forms sparse and tiny nanofibers. After incubating for 72 h, the average diameter of the sparse and tiny nanofibers is 3.7 nm (Figure 3B,G). To further investigate the self-assembly of **Pro-1P-NMe** after the addition of ACP, we examined time-dependent morphology changes by negative-staining TEM. The results reveal the growth of nanofibers at pH 5.0 upon addition of ACP. Specifically, 1 h after the addition of ACP we can only observe sparse nanofibers with diameters of 4.0 nm (Figures 3D and S30). The nanofibers grow to several micrometers in length and become entangled with each other to form a nanofibrous network after 5 h co-incubation with ACP (Figure 3E). The nanofibrous network keeps growing and remains the same after incubation for 24 h (or longer) with an average fiber diameter of 6.7 nm (Figures 3C, F, H and S31). These results indicate that the self-assembly of **Pro-1P-NMe** occurs concomitantly with the hydrolysis with ACP at pH 5.0 (Figure 2B), thus validating that the formation of the nanofibrous network can only be achieved by acid catalysis upon addition of ACP. The difference in the nanofiber diameter and density between these two stages suggested our system had a multistage nature. The CD spectrum of **Pro-1P-NMe** when incubated in aqueous solution (pH 7.4 and 5.0) exhibits one negative and positive band located at $\lambda = 190$ nm and 208 nm (Figure S32). However, the signal intensity reduces significantly and changes into one positive and two negative bands at $\lambda = 187$ nm, 200 nm, and 228 nm during the ACP-instructed self-assembly. The results reveal the transformation after acid-catalyzed hydrolysis, further demonstrating the multistage self-assembly of **Pro-1P-NMe**.

To demonstrate the concept of controlling nanofiber formation in cellular milieu, we chose human osteosarcoma cells (Saos-2), which express high levels of extracellular phosphatase, as a model cell line.[17] As shown in Figure 4A, the cells incubated with **1P** exhibit green fluorescence on the cell surface, which suggests that the phosphatase of the cell surface hydrolyze **1P** to form enzymatic assemblies, which is further verified by HPLC (Figure S33). This result is also consistent with the recent reports of using ectophosphatase to induce molecular self-assembly on cell surfaces,[18] which is in agreement with the non-substrate specificity of phosphatase, which limits its further applications. In contrast, we could only observe the green fluorescence of assemblies in the lysosome

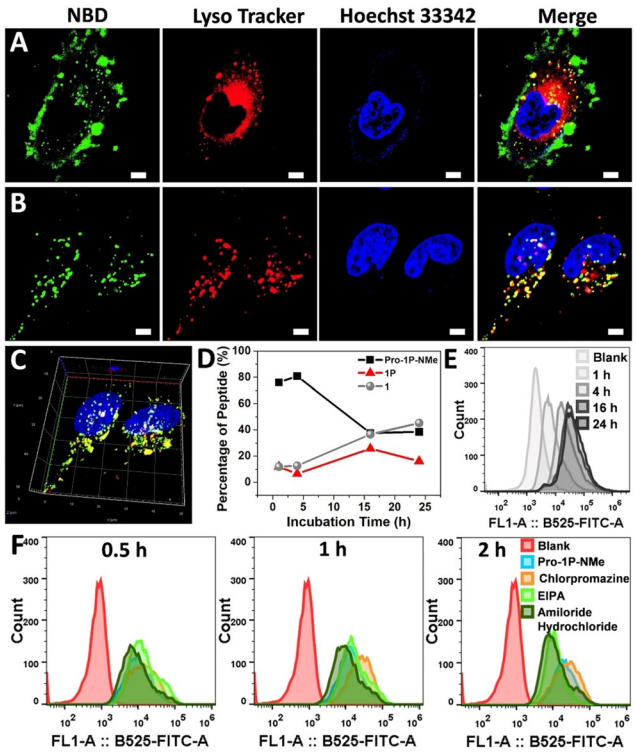

Figure 4. CLSM images of Saos-2 cells incubated with A) **1P** (100 μM) and B) **Pro-1P-NMe** (100 μM) for 4 h and C) 3D construction from (B). Scale bar is 5 μm. D) Percentage of the molecular species in cells after incubating **Pro-1P-NMe** with Saos-2 cells for different times. E) Flow cytometry results of Saos-2 cells incubated with **Pro-1P-NMe** (100 μM) for 1 h, 4 h, 16 h, and 24 h. F) Flow cytometry analysis of Saos-2 cells treated with **Pro-1P-NMe** (0.5 h, 1 h, and 2 h) in the absence or presence of the different inhibitors (chlorpromazine (50 μM), EIPA (5 μM), and amiloride hydrochloride (50 μM)). Each experiment was repeated three times.

of Saos-2 cells after treating with **Pro-1P-NMe** (4 h), as evident from co-localization with lysosome tracker (Figure 4B, C, red color). Time-dependent HPLC analysis (Figure S35 and Table S3) of the molecular transformation in cells reveals that **Pro-1P-NMe** could be recognized easily by acid phosphatase in acidic lysosomes after transforming to **1P** through acid-catalyzed hydrolysis. We collected the cell lysate and quantified the relative conversion in cells after incubating **Pro-1P-NMe** with Saos-2 cells for different times. The results show that **Pro-1P-NMe** transforms into **1P** and **1** incrementally, with 45.3% conversion after 24 h (Figure 4D). In addition, time-dependent CLSM experiments showed that the fluorescence from the self-assembled molecules increased gradually (Figure S34), which suggests that the accumulation of the assemblies in the lysosome is a time-dependent enzymatic process rather than a spontaneous self-assembly in the lysosomes. We also observed fluorescence in the cytoplasm, which indicates that the assemblies could escape from the endosome as the incubation time increased. Moreover, the fluorescent assemblies in the lysosome can also be passed to the new divided cells (Figure S36), which further demonstrate that the cell division was not influenced by the self-assembly of **Pro-1P-NMe** in the lysosome. To further investigate the time-dependent cellular accumulation of assemblies, we also used flow cytometry to characterize the fluorescence of assemblies in live cells. The results show that the intensity of the fluorescence from assemblies increases gradually over time (Figure 4E), thus suggesting the time-dependent formation of assemblies inside cells.

Furthermore, we also studied the endocytosis pathways of **Pro-1P-NMe** by flow cytometry (Figure 4F). Chlorpromazine, a clathrin-mediated endocytosis inhibitor, hardly affects the cellular uptake of **Pro-1P-NMe** during the tested period (2 h). However, the addition of EIPA and amiloride hydrochloride (macropinocytosis inhibitors) reduces the uptake of **Pro-1P-NMe** by about 55% and 56%, respectively. These results indicate that **Pro-1P-NMe** mainly undergoes micropinocytosis-mediated endocytosis.

We also used the nonspecific ACP inhibitors[19] NaF and Na_3O_4V for co-incubation with **Pro-1P-NMe**. The results show that both inhibitors significantly impede the formation of nanofibers in living cells (Figure 5A–D), as evident by the

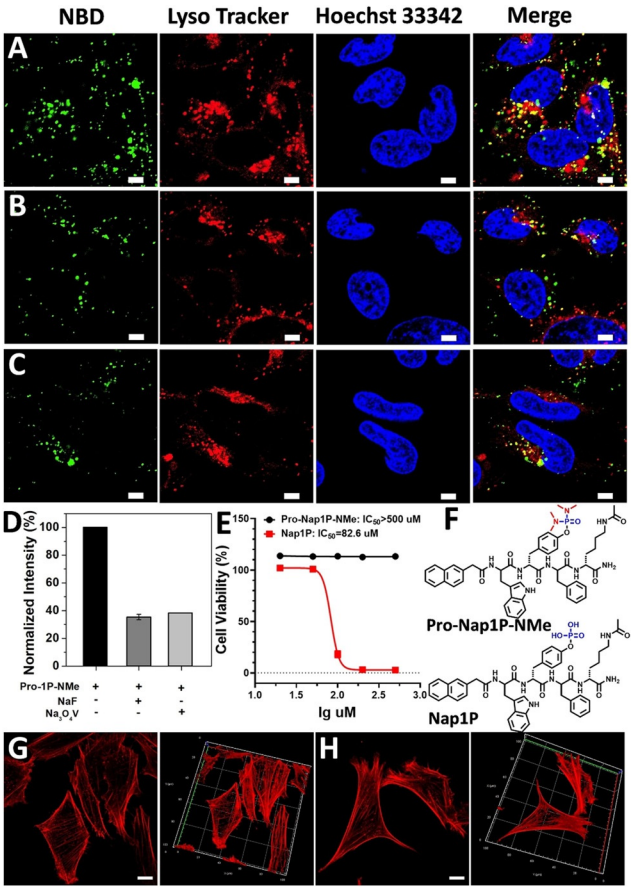

Figure 5. CLSM image of Saos-2 cells incubated with A) **Pro-1P-NMe** and in the presence of B) NaF and C) Na_3O_4V. The concentrations of **Pro-1P-NMe**, NaF, and Na_3O_4V is 100 μM, 20 μM, and 20 μM, respectively. The scale bar is 5 μm. D) The fluorescence intensity of **Pro-1P-NMe** incubated with phosphatase inhibitors NaF and Na_3O_4V. E) Cytotoxicity of **Pro-Nap1P-NMe** and **Nap1P** against Saos-2 cells after 48 h. Naphthylacetic acid was used instead of NBD to test the cytotoxicity. F) Molecular structures of **Pro-Nap1P-NMe** and **Nap1P**. CLSM images and 3D construction of Saos-2 cells after incubating with G) culture medium and H) **Pro-1P-NMe** for 4 h. F-actin is stained with phalloidine (red). The scale bar is 10 μm.

reduction in the fluorescent intensity to 63.2 % (for NaF) and 61.6 % (for Na_3O_4V), respectively. We next investigated the biocompatibility of our strategy to Saos-2 cells. Since **Pro-1P-NMe** and **1P** contain fluorophore-NBD, the absorbance of NBD could interfere with the absorbance of MTT, thus we synthesized analogues of **Pro-1P-NMe** and **1P** by replacing NBD by a naphthtyl group (Nap) to yield Nap-^{D}Wp^{D}Y-$(NMe_2)_2$^{D}F^{D}K(Ac)-NH_2 (**Pro-Nap1P-NMe**) and Nap-^{D}Wp^{D}Y^{D}F^{D}K(Ac)-NH_2 (**Nap1P**; Figures S5–8, S17, S18). The MTT results show that the IC_{50} value of **Pro-Nap1P-NMe** is higher than 500 μM against Saos-2 cells, while **Nap1P** exhibits much higher cytotoxicity, with a IC_{50} value of 51.8 μM (Figure S37). The CCK-8 assay—a more reliable assay to evaluate cell viability—further demonstrated the influence of **Pro-Nap1P-NMe** on cell fate. At a higher concentration of **Pro-Nap1P-NMe** (500 μM), the cell viability is comparable with the control group (treated with culture medium), while the IC_{50} value of **Nap1P** against Saos-2 cells is 82.6 μM (Figures 5 E, F, S38). Moreover, after treating **Pro-1P-NMe** for 4 h and 24 h, the F-actin of Saos-2 exhibits stretched thin actin filaments (Figures 5 G,H, S39), which indicates **Pro-1P-NMe** does not influence the cell morphology. These results together suggest the biocompatibility of our strategy for site-specific self-assembly in living cells. This is very important, since most of the phosphorylated peptides enter cells poorly and could only self-assemble on the cell surface where they show cytotoxicity, which hinders their further application in exploring biological functions of tyrosine phosphorylation at specific locations.

To directly investigate the formation of the assemblies in a cellular environment and visualize their cellular location, we employed Bio-TEM to image the high-pressure frozen and

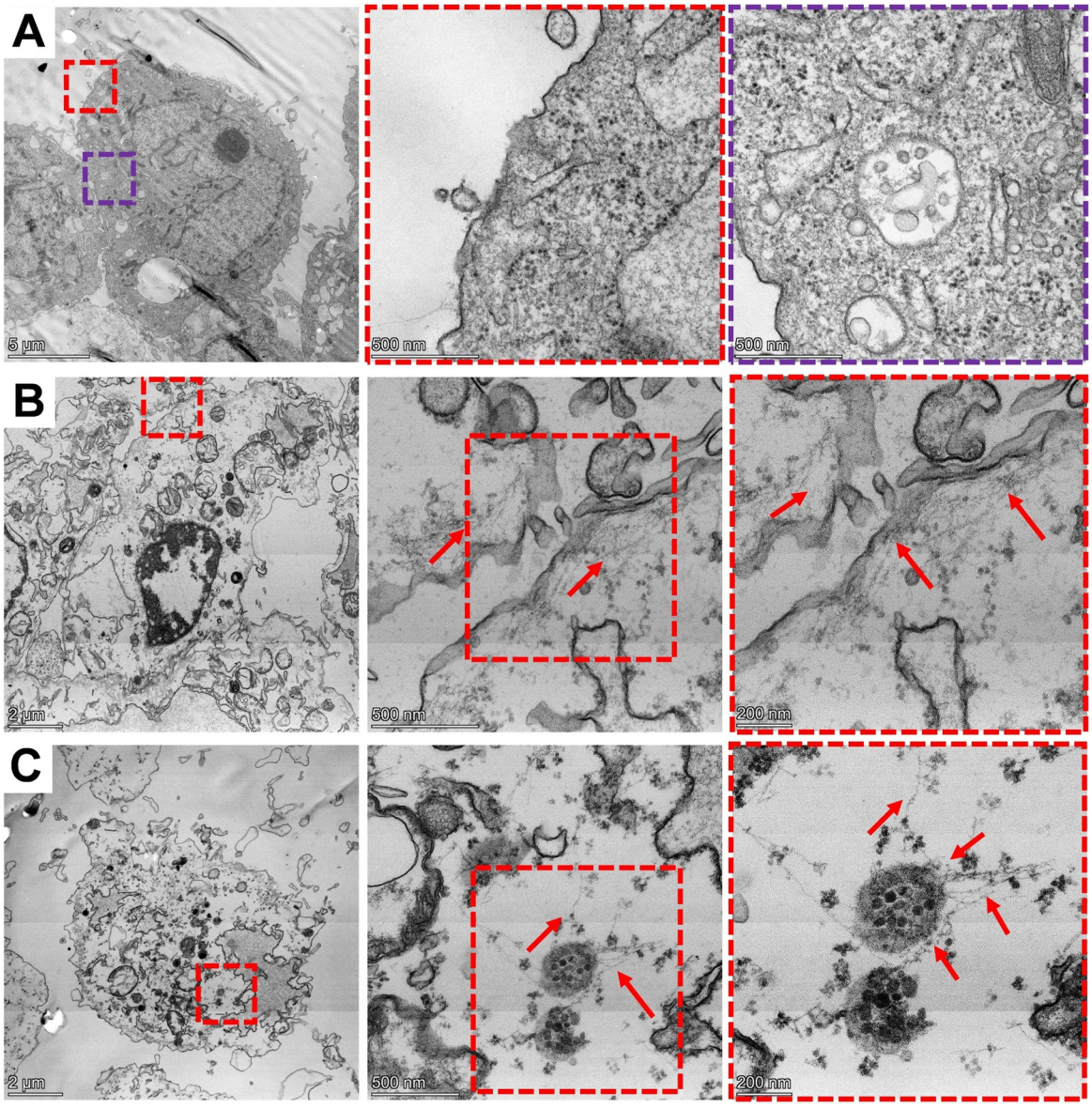

Figure 6. Electron microscopy images of filament formation by peptides inside the cells. Bio-EM image of A) a whole Saos-2 cell (untreated), B) a representative Saos-2 cell treated with **1P** (50 μM, 24 h), and C) a representative Saos-2 cell treated with **Pro-1P-NMe** (100 μM, 24 h). The red and purple boxes show the corresponding higher-magnification electron micrographs.

freeze-substituted Saos-2 cells. Compared with the case of untreated cells (Figure 6A), **1P**-treated Saos-2 cells exhibit bundles of nanofibers (Figure 6B), which spread from the outer plasma membrane to the inner plasma membrane. We hardly observe any filament formation inside the cells (Figure S40). In contrast, entangled filaments appear abundantly inside the cells after treatment with **Pro-1P-NMe** (Figures 6C and S41). Interestingly, most intracellular fibers are in proximity to lysosome or inside the lysosome. To further validate the intracellular formation of nanofibrous assemblies, we collected the cell lysate of samples treated with **Pro-1P-NMe** or untreated and analyzed them by TEM. The results show that aggregates of the nanofibers formed in the Saos-2 cells treated with **Pro-1P-NMe** (Figure S42) and has a similar morphology to those observed in Bio-TEM images. These results further demonstrate the self-assembly of **Pro-1P-NMe** inside the cells. To the best of our knowledge, this is the first direct observation of controlling filament formation inside the lysosome by enzymatic hydrogelation. These results, which agree with the observation from the CLSM experiments, strongly support our concept (Figure 1C).

To further demonstrate the importance of acid-catalyzed hydrolysis in multistage self-assembly in vitro and in living cells, we designed a nonhydrolyzable analogue—the diethyl phosphonate modified peptide NBD-^{D}Wp^{D}Y$(OEt)_2$^{D}F^{D}K-(Ac)-NH_2 (**Pro-1P-OEt**; Scheme S3 and Figures S9, S10, and S19). After obtaining **Pro-1P-OEt**, we first tested the stability of **Pro-1P-OEt** under physiological conditions in vitro. The LC-MS spectra show that there is no degradation of **Pro-1P-OEt** after 72 h incubation in aqueous buffer at pH 7.4 and pH 5.0 regardless of the presence of ALP or ACP (Figures 7A,B and S43), which indicates that **Pro-1P-OEt** is a suitable nonhydrolyzable analogue of **Pro-1P-NMe**. We next incubated Saos-2 cells with **Pro-1P-OEt** using the same procedure as for **Pro-1P-NMe**. As shown in Figure 7D, we only observed strong green fluorescence on the cell surface (Figure 7D), which differs from the results seen with **1P** and **Pro-1P-NMe**. The distribution of **Pro-1P-OEt** is not homogeneous around the cell surface. To better understand the reason for this phenomenon, we investigated the self-assembly of **Pro-1P-OEt** under physiological conditions. The TEM images revealed that the **Pro-1P-OEt** could self-assemble into

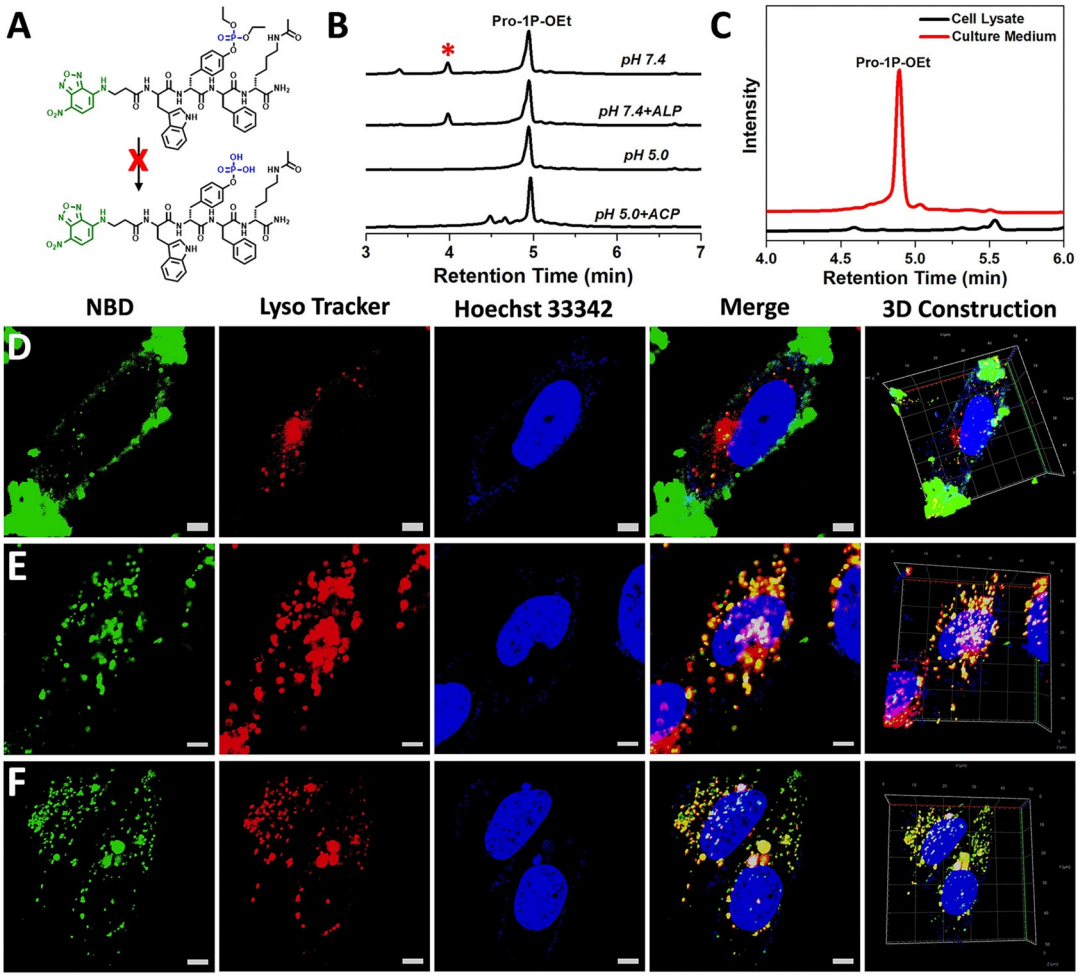

Figure 7. A) Molecular structures of **Pro-1P-OEt** and **1P**. B) HPLC spectra of **Pro-1P-OEt** after incubating with ALP (3.0 U mL^{-1}) and ACP (0.1 U mL^{-1}) in aqueous solution at different pH values. The molecular weight of the peak marked with an asterisk is shown in Figure S43. C) HPLC spectra of the cell lysate and the supernatants of the culture medium of **Pro-1P-OEt**-treated Saos-2 cells. CLSM images and 3D construction of Saos-2 cells incubated with D) **Pro-1P-OEt**, E) **Pro-2P-NMe**, and F) **Pro-3P-NMe** for 4 h. The concentration of **Pro-1P-OEt**, **Pro-2P-NMe**, and **Pro-3P-NMe** is 100 μM. The scale bar is 5 μm.

short and thin nanofibers (Figure S44). Considering the poor solubility of **Pro-1P-OEt** in aqueous solution, we speculated that the short nanofibers precipitated on the cell surface and could interact with the hydrophobic domain of the cell membrane in a nonspecific manner, thereby resulting in nonhomogeneous aggregates on the cell surface. We also used LC-MS to quantify the molecular species in the cell lysate and supernatants of the culture medium after incubating **Pro-1P-OEt** with Saos-2 cells. In the supernatants of the culture medium, the molecules of **Pro-1P-OEt** remain unchanged (Figure 7C), which is consistent with the enzymatic hydrolysis experiments in vitro. Moreover, we could barely observe the molecular composition in the cell lysate because of the low concentration of **Pro-1P-OEt** inside the cells. These results, together with previous investigations of **Pro-1P-NMe**, suggest the crucial role of the acid-catalyzed process in precisely controlling the enzyme-instructed self-assembly in living cells.

Furthermore, to demonstrate the universality of our strategy we synthesized NBD-^{D}W^{D}Fp^{D}Y$(NMe_2)_2$^{D}K(Ac)-NH_2 (**Pro-2P-NMe**) and NBD-^{D}pY$(NMe_2)_2$^{D}W^{D}F^{D}K(Ac)-NH_2 (**Pro-3P-NMe**; Figures S11–S14, S20, and S21), then investigated the cellular distribution of these peptides inside the Saos-2 cells. The CLSM images show that the variation of the sequence led to a similar phenomenon. As shown in Figure 7E, F, the green fluorescence of the assemblies was co-localized with the red fluorescence from the lysosome tracker, thereby demonstrating the robust nature of our strategy. These results, together with the above observations, suggest the critical role of the phosphoramidate group in the formation of enzyme-controlled assemblies in living cells.

Conclusion

In summary, this work describes an acid-activatable chemical approach to control enzymatic self-assembly in vitro and in live cells in a spatiotemporally controlled manner. The integration of acid-catalyzed hydrolysis and enzyme-induced self-assembly could be applied to any scenarios in which the phosphoramidate group is hydrolyzed under acidic conditions that express ACP. In addition to the formation of nanofibers inside the lysosome of Saos-2 cells, **Pro-1P-NMe** exhibits similar activity towards the PC-3 cell line, which overexpresses ACP. Time-dependent CLSM and Bio-TEM experiments clearly verified the formation of nanofibers in the lysosome of PC-3 cells (Figures S45–S47). Analysis of the molecular transformation in cell milieu also demonstrates the multistep self-assembly pathway of **Pro-1P-NMe** in PC-3 cells, thus implying the general utility of our strategy for the site-specific formation of molecular assemblies inside living cells. The established design strategy detailed herein would also be applicable to other systems for controlling nanostructure formation in specific locations, whereby the acid-catalyzed motif as well as the types of enzyme could be replaced.[5h,20]

Acknowledgements

This project was supported by the Foundation of Westlake University and Tencent Foundation, the National Natural Science Foundation of China (82022038), and the China Postdoctoral Science Foundation (2020M681930). We thank the Instrumentation and Service Center for Physical Sciences, Molecular Sciences, and Biomedical Research Core Facilities at Westlake University for the assistance with measurements.

Conflict of Interest

The authors declare no conflict of interest.

Keywords: enzymes · hydrogels · living cells · nanofibers · self-assembly

[1] a) G. M. Whitesides, B. Grzybowski, *Science* **2002**, *295*, 2418–2421; b) T. Aida, E. W. Meijer, S. I. Stupp, *Science* **2012**, *335*, 813–817.

[2] a) R. V. Ulijn, A. M. Smith, *Chem. Soc. Rev.* **2008**, *37*, 664–675; b) J. Raeburn, A. Zamith Cardoso, D. J. Adams, *Chem. Soc. Rev.* **2013**, *42*, 5143–5156; c) G. L. Liang, H. J. Ren, J. H. Rao, *Nat. Chem.* **2010**, *2*, 54–60; d) W. Tanaka, H. Shigemitsu, T. Fujisaku, R. Kubota, S. Minami, K. Urayama, I. Hamachi, *J. Am. Chem. Soc.* **2019**, *141*, 4997–5004; e) M. T. He, J. B. Li, S. Tan, R. Z. Wang, Y. Zhang, *J. Am. Chem. Soc.* **2013**, *135*, 18718–18721; f) D. J. Smith, G. A. Brat, S. H. Medina, D. Tong, Y. Huang, J. Grahammer, G. J. Furtmuller, B. C. Oh, K. J. Nagy-Smith, P. Walczak, G. Brandacher, J. P. Schneider, *Nat. Nanotechnol.* **2016**, *11*, 95–102.

[3] "Enzymes": J. F. Kennedy, J. F. Kennedy, *Carbohydrate Chemistry*, *Vol. 14* (Ed.: J. F. Kennedy), Royal Society of Chemistry, London, **1983**, pp. 230–344.

[4] a) Z. Yang, G. Liang, B. Xu, *Acc. Chem. Res.* **2008**, *41*, 315–326; b) Z. Feng, H. Wang, F. Wang, Y. Oh, C. Berciu, Q. Cui, E. H. Egelman, B. Xu, *Cell Rep. Phys. Sci.* **2020**, *1*, 100085; c) Z. Feng, H. Wang, X. Chen, B. Xu, *J. Am. Chem. Soc.* **2017**, *139*, 15377–15384.

[5] a) R. A. Pires, Y. M. Abul-Haija, D. S. Costa, R. Novoa-Carballal, R. L. Reis, R. V. Ulijn, I. Pashkuleva, *J. Am. Chem. Soc.* **2015**, *137*, 576–579; b) A. Tanaka, Y. Fukuoka, Y. Morimoto, T. Honjo, D. Koda, M. Goto, T. Maruyama, *J. Am. Chem. Soc.* **2015**, *137*, 770–775; c) J. Zhan, Y. B. Cai, S. S. He, L. Wang, Z. M. Yang, *Angew. Chem. Int. Ed.* **2018**, *57*, 1813–1816; *Angew. Chem.* **2018**, *130*, 1831–1834; d) M. Pieszka, S. Han, C. Volkmann, R. Graf, I. Lieberwirth, K. Landfester, D. Y. W. Ng, T. Weil, *J. Am. Chem. Soc.* **2020**, *142*, 15780–15789; e) Z. Q. Q. Feng, H. M. Wang, R. Zhou, J. Li, B. Xu, *J. Am. Chem. Soc.* **2017**, *139*, 3950–3953; f) Z. Zheng, P. Y. Chen, M. L. Xie, C. F. Wu, Y. F. Luo, W. T. Wang, J. Jiang, G. L. Liang, *J. Am. Chem. Soc.* **2016**, *138*, 11128–11131; g) L. L. Li, S. L. Qiao, W. J. Liu, Y. Ma, D. Wan, J. Pan, H. Wang, *Nat. Commun.* **2017**, *8*, 1276; h) L. L. Lock, C. D. Reyes, P. C. Zhang, H. G. Cui, *J. Am. Chem. Soc.* **2016**, *138*, 3533–3540.

[6] a) L. Yadav, F. Tamene, H. Goos, A. van Drogen, R. Katainen, R. Aebersold, M. Gstaiger, M. Varjosalo, *Cell Syst.* **2017**, *4*, 430–444; b) J. F. Shi, G. Fichman, J. P. Schneider, *Angew. Chem. Int. Ed.* **2018**, *57*, 11188–11192; *Angew. Chem.* **2018**, *130*, 11358–11362.

[7] a) Y. Kuang, J. F. Shi, J. Li, D. Yuan, K. A. Alberti, Q. B. Xu, B. Xu, *Angew. Chem. Int. Ed.* **2014**, *53*, 8104–8107; *Angew. Chem.*

2014, *126*, 8242 – 8245; b) Z. M. Yang, K. M. Xu, Z. F. Guo, Z. H. Guo, B. Xu, *Adv. Mater.* **2007**, *19*, 3152 – 3156.
[8] a) Z. Q. Q. Feng, H. M. Wang, S. Y. Wang, Q. Zhang, X. X. Zhang, A. A. Rodal, B. Xu, *J. Am. Chem. Soc.* **2018**, *140*, 9566 – 9573; b) F. Versluis, D. M. van Elsland, S. Mytnyk, D. L. Perrier, F. Trausel, J. M. Poolman, C. Maity, V. A. A. le Sage, S. I. van Kasteren, J. H. van Esch, R. Eelkema, *J. Am. Chem. Soc.* **2016**, *138*, 8670 – 8673; c) M. T. Jeena, L. Palanikumar, E. M. Go, I. Kim, M. G. Kang, S. Lee, S. Park, H. Choi, C. Kim, S. M. Jin, S. C. Bae, H. W. Rhee, E. Lee, S. K. Kwak, J. H. Ryu, *Nat. Commun.* **2017**, *8*, 26.
[9] X. Z. Luo, G. S. Fu, R. S. E. Wang, X. Y. Zhu, C. Zambaldo, R. H. Liu, T. Liu, X. X. Lyu, J. T. Du, W. M. Xuan, A. Z. Yao, S. A. Reed, M. C. Kang, Y. H. Zhang, H. Guo, C. H. Huang, P. Y. Yang, I. A. Wilson, P. G. Schultz, F. Wang, *Nat. Chem. Biol.* **2017**, *13*, 845 – 849.
[10] S. R. Bonam, F. Wang, S. Muller, *Nat. Rev. Drug Discovery* **2019**, *18*, 923 – 948.
[11] H.-G. Chao, B. Leiting, P. D. Reiss, A. L. Burkhardt, C. E. Klimas, J. B. Bolen, G. R. Matsueda, *J. Org. Chem.* **1995**, *60*, 7710 – 7711.
[12] S. S. Hassan, H. E. Sayour, A. H. Kamel, *Anal. Chim. Acta* **2009**, *640*, 75 – 81.
[13] J. Karanicolas, J. E. Com, I. Chen, L. A. Joachimiak, O. Dym, S. H. Peck, S. Albeck, T. Unger, W. X. Hu, G. H. Liu, S. Delbecq, G. T. Montelione, C. P. Spiegel, D. R. Liu, D. Baker, *Mol. Cell* **2011**, *42*, 250 – 260.
[14] Y. Gao, J. F. Shi, D. Yuan, B. Xu, *Nat. Commun.* **2012**, *3*, 1033.
[15] L. Bialy, H. Waldmann, *Angew. Chem. Int. Ed.* **2005**, *44*, 3814 – 3839; *Angew. Chem.* **2005**, *117*, 3880 – 3906.
[16] B. A. Webb, M. Chimenti, M. P. Jacobson, D. L. Barber, *Nat. Rev. Cancer* **2011**, *11*, 671 – 677.
[17] C. Pautke, M. Schieker, T. Tischer, A. Kolk, P. Neth, W. Mutschler, S. Milz, *Anticancer Res.* **2004**, *24*, 3743 – 3748.
[18] Z. Q. Q. Feng, T. F. Zhang, H. M. Wang, B. Xu, *Chem. Soc. Rev.* **2017**, *46*, 6470 – 6479.
[19] H. Hamba, T. Nikaido, G. Inoue, A. Sadr, J. Tagami, *J. Dent.* **2011**, *39*, 405 – 413.
[20] a) Z. J. Hai, J. L. Wu, D. Saimi, Y. H. Ni, R. B. Zhou, G. L. Liang, *Anal. Chem.* **2018**, *90*, 1520 – 1524; b) S. S. He, J. C. Li, Y. Lyu, J. G. Huang, K. Y. Pu, *J. Am. Chem. Soc.* **2020**, *142*, 7075 – 7082.

Manuscript received: July 21, 2021
Accepted manuscript online: September 2, 2021
Version of record online: October 1, 2021

